The splicing factor kinase SRPK1 is a therapeutic target for Peripheral Vascular Disease

[1]Sohni Ria Bhalla, [1]Mussarat Wahid, [1]Jason Amartey, [1]Federica Riu, [1]Yizhuo Gao, [1]Jyoti Agrawal, [1]Amy P Lynch, [1]Maria JC Machado, [2]Tom Hawtrey, [3]Ryosuke Kikuchi, [1]Kathryn R Green, [4]Lydia Teboul, [1]Claire Allen, [1]Zoe Blackley, [1]Keerthana Rajaji, [1]Daisy Marsden, [1]Jennifer Batson, [5]Steven J Harper, [6]Sebastian Oltean, [7]Winfried Amoaku, [1]Andrew V Benest, [2]Jonathan Morris, [8]Bruce Braithwaite, [1]David O Bates.

[1]Tumour and Vascular Biology Laboratories, Division of Cancer and Stem Cells, Centre for Cancer Sciences, School of Medicine, Biodiscovery Institute, University of Nottingham, Science Road, NG7 2RD.

[2]School of Chemistry, University of New South Wales, Sydney, Australia.

[3]Division of Clinical Laboratory, Gifu University Hospital, 1-1 Yanagido, Gifu, 501-1194, Japan.

[4]Mary Lyon Centre, MRC Harwell Institute, Harwell Campus, Oxfordshire, OX11 0RD, UK.

[5]Division of Nephrology, North Bristol NHS Trust, Southmead Hospital, Bristol

[6] Department of Clinical and Biomedical Sciences, Medical School Building, St Luke's Campus, Magdalen Road, Exeter, EX1 2LU, UK

[7]Department of Ophthalmology, School of Medicine, University of Nottingham, Queen's Medical Centre, Nottingham, NG7 2UH.

[8]Department of Vascular Surgery, Nottingham University Health Care Trust, Queen's Medical Centre, Nottingham, NG7 2UH.

Abstract

Introduction. VEGF-A splicing has been shown to be regulated in epithelial cells and cancer cells by the phosphorylation of serine/arginine splicing factor 1 (SRSF1) by serine-arginine protein kinase 1 (SRPK1). In these cell types inhibition of SRPK1 switches splicing to the anti-angiogenic VEGF-A isoforms. In peripheral arterial disease (PAD) vascular insufficiency and reduced blood flow results from overexpression of the anti-angiogenic isoform of VEGF-A, VEGF-A_{165}b, in circulating monocytes**.** To determine if SRPK1 was involved in VEGF expression by monocytes driving impaired collateral vessels, we investigated the effects of SRPK1 inhibition and monocyte specific SRPK1 knockout in mouse models of PAD and in human monocytes from patients with PAD.

Methods. VEGF-A_{165}b activity was measured in monocytes from patients with PAD by co-culture with endothelial cells in a migration assay in the presence of SRPK1 inhibitors. Mice with impaired revascularisation due to either soluble frizzled related protein 5 knockout (Sfrp5$^{-/-}$), monocyte specific gain of function of Wnt5a (LysM-Wnt5a^{GOF}), or obese mice on a high fat high sucrose (HF/HS) diet were subjected to left femoral artery ligation and treated with SRPK1 inhibitor SPHINX31. To determine monocyte specific SRPK1 activity we generated an SRPK1 conditional knockout under the control of a monocyte specific (LysM-Cre) driver (SRPK1^{MoKO}) mice. Blood flow to the paw was measured by Laser Speckle Imaging before, and for 28 days after, surgery.

Results. Monocytes from patients with PAD significantly inhibited migration of human endothelial cells in culture, which was inhibited by an anti-VEGF-A_{165}b antibody. Surprisingly, this inhibition was reversed by SRPK1 inhibition, which switched splicing from VEGF-A_{165}b to VEGF-A_{165}a. In the Sfrp5$^{-/-}$, LysM-Wnt5a^{GOF} and HF/HS mouse models of PAD, impaired blood flow was reversed by SRPK1 inhibition. The impaired revascularisation in LysM-Wnt5a^{GOF} mice was also rescued in LysM-Wnt5a^{GOF}: SRPK1^{MoKO} mice. Impaired blood flow recovery was also rescued in obese-SRPK1^{MoKO} mice.

Conclusion. VEGF splicing in monocytes is differently regulated from VEGF splicing in epithelial cells or cancer cells. This indicates that control of splicing is dependent on

63 cell type and/or environment. SRPK1 inhibition is able to enhance collateralisation in
64 mice, and in vitro models of monocyte dependent impaired angiogenesis in human
65 endothelial cells.
66

Introduction

More than 4 million people in the UK have diabetes (7.9% of the population), predominantly type 2 (T2D). This is predicted to rise by 20% by 2030 (data from APHO Diabetes Prevalence Model). Progressive atherosclerosis and microvascular disease are the leading causes of amputations and are most common in people with diabetes. However, in otherwise healthy individuals, progressive atherosclerosis and microvascular disease can be circumvented by the development of collateral vessels. This collateral formation is impaired in people with diabetes, resulting in more severe PAD, critical limb threatening ischemia (CLTI) and ischemia of other tissues, including coronary vascular disease (CVD), leading to increased incidence of fatal myocardial infarction (MI)[1]. Understanding why diabetes impairs collateral formation, and identifying ways that can overcome that inhibition, could provide radical, effective new therapies for people with diabetes, PAD and CVD.

Hyperactivation of the Wnt5a pathway in monocytes has been proposed to be a key mechanism through which metabolic syndrome patients[2] have impaired collateralisation[3-5]. In T2D and in obesity circulating monocytes are pro-inflammatory[6]. These circulating monocytes have increased VEGF production[7], suggesting that they should be able to aid arteriogenesis and angiogenesis and stimulate collateral formation. However, the monocytes appear unable to elicit the actions of VEGF[8]. This paradox – increased VEGF production but reduced angiogenic capability in diabetic patients – may be partly explained by findings that monocytes from T2D patients, and mouse and rat models of T2D, have increased Wnt5a expression and activity[4]. Sfrp5, the endogenous inhibitor of Wnt5a is reduced in plasma from patients with obesity, T2D or both[9,10]. The effect of Sfrp5 knockout on angiogenesis in adult mice is significantly impaired recovery of blood flow and angiogenesis after hind limb ischemia (HLI), a model of collateralisation in mice. This impairment is reproduced by a Wnt5a overexpressing monocytic lineage-specific gain of function animal (LysM-Wnt5a^{GOF}). VEGF-A mRNA and protein levels are dramatically upregulated in these animals, contrary to the findings of reduced angiogenesis[5].

VEGF-A exists as two functionally contrasting families of isoforms resulting from mRNA processing[11]. Alternative 3' splice site selection in the terminal exon, exon 8, can generate either pro-angiogenic isoforms termed VEGF-A$_{xxx}$a where xxx is the

number of amino acids in the mature polypeptide (e.g. VEGF-A_{165}b), or isoforms that can inhibit angiogenesis by use of a splice site 66 nucleotides downstream of the proximal 3' splice site, termed VEGF-A_{xxx}b[12]. VEGF-A_{165}b is the most studied member of this family. VEGF-A_{165}b acts as a partial agonist for its receptors[13-15], inhibiting VEGF-A_{165}a induced angiogenesis[15], but protecting endothelial and epithelial cells (including ocular and renal epithelial cells) from cytotoxic insults[16,17]. VEGF-A_{165}b binds to the tyrosine kinase receptors VEGFR1 and VEGFR2[13-15] but not neuropilin or heparan sulphate proteoglycans[14] resulting in partial activation of VEGFR2[18], unstable kinase activation due to lack of phosphorylation of Tyr1054 in VEGFR2[13] and inhibition of VEGFR1 signalling[19].

Interestingly, the impaired revascularisation seen in sfrp5$^{-/-}$ and LysM-Wnt5a^{GOF} mice is $VEGF_{xxx}$b dependent as $VEGF_{xxx}$b neutralising antibodies reversed the blocked revascularisation[5]. Moreover, VEGF-A_{165}b is upregulated in mouse obesity models, and VEGF-A_{165}b selective antibodies improved collateralisation in models of both peripheral ischemia[5,19-21] and coronary vascular disease[22]. $VEGF_{165}$b has also been shown to be upregulated in people with peripheral arterial disease and in people with coronary vascular disease[23], both at the RNA level in circulating monocytes[5], and at the protein level in plasma[22], muscle and macrophages[5]. These results provide a potential explanation for impaired collateral formation in diabetes, and a potential novel therapeutic strategy to reduce cardiovascular disease in diabetic patients. That strategy would require selective inhibition of VEGF-A_{165}b in monocytes in people with diabetes and ischemia**.** Pre-mRNA splicing is orchestrated by splicing factors. In contrast with constitutive splicing, alternative splicing refers to the recruitment of a unique pattern of splicing factors (tissue and developmental stage-specific) resulting in transcripts that encode different proteins, often with contrasting properties. The actions of key splicing factors (SFs) such as the SR proteins SRSF1 and SRSF6 can be modulated by small molecular weight inhibitors of their specific kinases SRPK1/2 (e.g. SPHINX31[24]) and CLKs (e.g. TG003)[25]. SRSFs are known to affect VEGF-A splicing – in epithelial cells, SRSF6 over-expression switches expression to VEGF-A_{165}b[26], and SRSF1 to VEGF-A_{165}a in kidney and ocular epithelial cells[27,28], and SRSF2 to VEGF-A_{165} in lung cancer cells[29]. In epithelial and cancer cells, inhibition of SRSF1 phosphorylation by SRPK1 blockade inhibits VEGF-A proximal splice site selection in exon 8[30,31], and SRPK1 inhibition is an effective anti-angiogenic strategy

135 for retinal neovascularisation and choroidal neovascularisation in eye disease[30,32,33].
136 However, we do not yet know what regulates VEGF splicing in monocytes, or whether
137 this holds true in monocytes from diabetic patients with cardiovascular disease, or
138 monocytes as they differentiate into macrophages during adherence and
139 extravasation.
140 We therefore investigated the mechanism of splicing control in monocytes, and
141 show that SRPK1 in monocytes, in contrast to epithelial cells, switches splicing to the
142 VEGF-A_{165}b isoform in monocytes, and SRPK1 inhibition is able to reverse peripheral
143 vascular disease in mice, and induce the angiogenic capability of human monocytes.
144

Methods

Patient samples

Patients with peripheral artery disease (ankle brachial pressure index <0.9) were enrolled from Queen's Medical Centre, Nottingham (UK) after obtaining their written informed consent. 50 mL of whole peripheral blood was collected in EDTA tubes. Peripheral blood mononuclear cells (PBMCs) were isolated from blood by density gradient centrifugation using Ficoll® Paque Plus (Cytiva, Marlborough, MA, USA). Blood was buffered by mixing it with an equal volume of PBS. 15mL of Ficoll-Paque Plus solution (Cytiva) in a 50 mL conical tube was carefully overlaid with 30 mL of diluted blood and centrifuged for 20 minutes at 1,000 g at room temperature with slow accelerator and no brake. The interface containing the cellular layer was collected from each tube with a transfer pipette, washed with PBS and placed into a 50 mL tube and centrifuged for 10 minutes at 600g with maximum acceleration and deceleration at room temperature. The obtained PBMCs were treated with 5mL of red blood cell lysis buffer (0.83g NH4Cl, 0.1g KHCO3, 5% EDTA dissolved in 100 mL of distilled water and filter sterilized using 0.22 μM filter) and incubated for 5 minutes at room temperature to lyse the remaining red blood cells. This tube containing lysed cells was then centrifuged for 6 minutes at 400g at room temperature. The PBS wash was repeated followed by centrifugation for 6 minutes at 400 g at room temperature, cell count and viability assessment were performed. To separate monocytes from the PBMCs, antihuman CD14 MicroBeads (Miltenyi Biotec, Bergisch Gladbach, Germany), were used as per manufacturer's protocol. The CD14 positive cells were then re-suspended in RPMI 1640 medium (Fisher Scientific, Leicester, UK) supplemented with 10% human AB serum (Zen Bio, Durham, NC, USA).

Endothelial cell migration assay

Human Umbilical Vein Endothelial Cell (HUVEC) (PromoCell GmbH, Heidelberg Germany) were serum starved overnight in Endothelial cell basal medium (ECBM) supplemented with endothelial cell growth kit (PromoCell GmbH, Heidelberg Germany) without serum. Transwell migration assays were performed in 24-well Thincert, (8.0μm pore size; Greiner Bio-One, GL, UK) placed in 24-well plates containing 0.1% fetal calf serum without or with 40ng/ml $VEGF_{165}a$, 40ng/ml $VEGF_{165}a$ and 40ng/ml $VEGF_{165}b$, or both isoforms and increasing concentrations of mouse anti-VEGF-$A_{165}b$ antibody[15], or in human AB serum (HSER-ABP100ML AMSBio, Oxford,

179 UK) in RPMI 1640 media (Fisher Scientific, Leicester, UK) alone (0.5% control), with
180 40ng/ml $VEGF_{165}a$ or with 40ng/ml $VEGF_{165}a$ $CD14^+$ labelled monocytes suspended
181 at a density of $5x10^4$ cells and treatments as shown. HUVEC were suspended in
182 serum-free ECBM (without supplements) and plated at a density of $5x10^4$ cells on the
183 upper chamber of the 8µm inserts. Endothelial cells were allowed to migrate overnight
184 at 37°C under 5.0% CO_2. The inserts were washed 3 times in PBS and fixed with 4%
185 paraformaldehyde (PFA) for 15 minutes. After fixation, inserts were washed 3 times in
186 PBS and stained with DAPI (nuclei stain) for 15 minutes at room temperature. Stained
187 membranes were removed from inserts and mounted on the glass slide. The migrated
188 cells were counted under a microscope in 3 different views away from the insert edge
189 by an observer blinded to treatment (10x magnification). Each monocyte sample was
190 reproduced in triplicate.
191
192 **Animal model.** $Sfrp5^{-/-}$ and LysM-$Wnt5a^{GOF}$ mice were a kind gift of K Walsh. Mice
193 with SRPK1 knockout were generated in collaboration at MRC Harwell by flanking
194 exon 7 of *Srpk1* gene with LoxP sites. The promoter driven L1L2-Bact-P cassette was
195 removed by crossing mice with flipase mediated recombination generating $SRPK1^{Fl/Fl}$
196 mice. To generate the SRPK1 knockout mouse model (hereafter referred to as
197 $SRPK1^{MoKO}$), the $Srpk1^{Fl/Fl}$ mice were crossed with Lysozyme M-Cre mice. To
198 generate the double transgenic mouse model (hereafter referred to as LysM-
199 $Wnt5a^{GOF}$: $SRPK1^{MoKO}$), the LysM-$Wnt5a^{GOF}$ mice were crossed with the $SRPK1^{Fl/Fl}$
200 mice. All mice were maintained on a C57/BLJ background. Mice were fed either a
201 normal chow diet (Teklad global, 2018S) or a HF/HS diet (Bio-Serv, S1850) as
202 indicated. The composition of the HF/HS diet was 35.8% fat, 36.8% carbohydrates
203 and 20.3% protein. For the HF/HS diet, mice were maintained on a HF/HS diet from
204 the age of 4 weeks old for the duration of the study.
205
206 **Hind limb ischemia surgical procedure.** All animal experiments were conducted in
207 accordance with the Animal Scientific Procedures Act (ASPA) of 1986 under a UK
208 Home Office License at the University of Nottingham Biological Services Unit. All
209 mixed gender transgenic C57/BLJ mice were subjected to unilateral hindlimb ischemia
210 between 10 to 12 weeks of age. Anaesthesia was induced with 2% isoflurane in 100%
211 oxygen at rate of 2L/min. Body temperature was controlled throughout using a
212 homeothermic blanket and rectal probe (Harvard Apparatus). The hair was removed

213 from the hind limb using Nair hair removal cream and sterilised using chlorohexidine-
214 based solution. Mice were administered a pre-operative analgesic, buprenorphine
215 (0.05mg/kg, subcutaneous) and saline solution (0.9% sodium chloride at 40ml/kg). An
216 incision was cut in the left medial thigh and the connective tissue was teased apart to
217 expose the femoral artery, vein and nerve. The nerve bundle and vein were teased
218 apart from the femoral artery. The femoral artery was ligated in two sites above and
219 below the epigastric branch and electro-coagulated in between to induce ischemia to
220 the left hind paw. The blood flow to both paws was measured using the laser speckle
221 imaging system (Moors FLIP2, Moors instruments). The blood flow was monitored on
222 pre-operative day 0 and post-operative days 0, 3, 7, 14, 21 and/or 28. The ratio of the
223 blood flow was calculated between the ischemic vs contralateral paw to measure the
224 blood flow recovery throughout the duration of the study. If the reduction in blood flow
225 was less than 70% the animals were excluded for subsequent analysis *a priori*. For
226 SPHINX31 *in vivo* treated experiments, animals were treated with 0.8mg/kg
227 SPHINX31 synthesised as described in [24] bi-weekly for the duration of the study.
228 Twenty $Sfrp5^{-/-}$ and twenty wild type mice were used, and 8 of each type treated with
229 Sphinx31. Two sfrp5-/- and one wild type animal were excluded due to lack of impaired
230 flow (as outlined above). Eight of each group were perfuse fixed for
231 immunofluorescence and four had protein extracted for VEGF assessment. In one wild
232 type animal protein was lost during processing.
233 Eighteen $Wnt5A^{GOF}$ mice were used, 9 in the control group and 9 in the Sphinx31
234 treated group. 2 mice were excluded from the $Wnt5A^{GOF}$ and one from the Sphinx31
235 group due to insufficient ligation.
236
237 **Immunofluorescent staining.** At the experimental end-point, mice euthanized by
238 cardiac perfusion with 4% PFA/PBS had gastrocnemius muscle collected. Tissue was
239 post fixed in 4% PFA/PBS overnight at 4°C, cryoprotected in 30% sucrose and
240 embedded in OCT. The muscles were cryosectioned into 5µm- thick sections and
241 stained for IB_4 (1:150, Sigma) and αSMA-Cy3 (1:300, Sigma). Sections were imaged
242 using a confocal microscope and fluorescent microscope.
243
244 **Isolation of CD11b mouse monocytes**. Freshly isolated bone marrow and spleen
245 from 10 to 12 weeks of age WT and $SRPK1^{MoKO}$ mice were used. Bone marrow
246 immune cells and splenocytes were exposed to red blood cell lysis. The remaining

247 cells were separated from a mixed population of cells to monocytes and non-
248 monocytes using the CD11b monocyte isolation kit (Miltenyi Biotech) following the
249 manufacturer's instructions using Miltenyi LS columns.
250
251 **Western blotting**
252 Mouse gastrocnemius muscle tissue samples obtained on postoperative day 7 were
253 homogenized in lysis buffer containing 20 mm Tris-HCl (pH 8.0), 1% Nonidet P-40,
254 150 mm NaCl, 0.5% deoxycholic acid, 1 mm sodium orthovanadate, and protease &
255 phosphatase inhibitor cocktail (Thermo Scientific). Protein content was determined by
256 the Bradford method. Equal amounts of protein lysates were resolved by SDS-PAGE.
257 The membranes were immunoblotted with the indicated antibodies (anti-SRPK1
258 antibody (ab38017), abcam, anti-SRSF6 antibody (ab244425), and anti-SRPK1,
259 HPA016431, Sigma Aldrich) at a 1:1000 dilution followed by the secondary antibody
260 conjugated to horseradish peroxidase at a 1:1000 - 5000 dilution. An ECL western
261 blotting Detection kit (Thermo Scientific) was used for detection. Immunoblots were
262 normalized to total loaded protein.
263
264 **Cell Lysis**

265 Protein was extracted from monocytes after treatment. Cells previously treated with
266 inhibitors were centrifuged at 10,000 RPM at 4°C untill a pellet was formed. Cell lysis
267 buffer (1xNP40, 1mM phenylmethylsulfonyl fluoride (PMSF), 10mM Sodium
268 orthovanadate (Na_3VO4), 1x Protease Inhibitor cocktail (Roche), 10mM sodium
269 fluoriude) was added to the pellet for 10 mins. The cell extract was vortexed for 15 sec
270 three times over a 10 min incubation on ice. Samples were centrifuged at 12,000 x g
271 for 10 min at 4oC and the supernatant was collected in a fresh Eppendorf and stored
272 at -80oC. Protein concentration was quantified using a Pierce BCA Protein Assay Kit
273 (Thermo Scientific 23225).

274 **ELISA**
275 High binding 96-well plates were coated with 100µl of either 0.75µg/ml hVEGF-A_{165}a
276 AbD24645 or 10µg/ml VEGF-A_{165}b capture antibody overnight at room temperature on
277 the shaker. The plates were washed three times with wash buffer (0.05% Tween-
278 20/PBS, T-PBS) and blocked twice with 300µl/well of Superblock and discarded

279 immediately. Serial dilutions were prepared with rhVEGF-A_{165}a and rhVEGF-A_{165}b
280 diluted in PBS (ranging from 1.95 to 4000pg/ml as well as a blank and a negative
281 control) were added in duplicate (100µl/well). 100µg of protein tissue was added in
282 duplicate to each well. The 96-well plates were incubated for two hours at room
283 temperature on a shaker. Then the 96-well plates were washed three times and
284 incubated with 100µl of detection antibody from kit diluted in 1% BSA/PBS for two
285 hours. After another wash step, 100µl/well of horseradish peroxidase (HRP)-
286 conjugated streptavidin (diluted according to kit in 1% BSA in PBS was added and the
287 plate was left in the dark for 30 minutes. After a final wash step, 100µl/well of the
288 substrate solution (Abcam) was incubated for 20 to 30mins at room temperature in the
289 dark. The reaction was stopped by the addition of 50µl/well of either 1M hydrochloric
290 acid or sulphuric acid. The colorimetric reaction was measured using the microplate
291 reader at 450nm with a 620nm reference (Infinite F50, Tecan UK). The protein
292 concentration in each sample was calculated by subtracting absorbance values from
293 the blank and the standard curves was used to calculate protein content in each
294 sample.
295
296 **PCR.** RNA was isolated from $CD11b^+$ and $CD11b^-$ cells using Trizol. 1µg RNA was
297 transcribed to cDNA using the Takara Primescript RT kit (Takara) as directed by the
298 manufacturer. Each 15µl consisted of 0.4uM primers, 2x GoTaq master mix (Promega)
299 and 1µl cDNA. The primer sequences for the target genes were: *Srpk1*: forward, 5'-
300 TCTCGCCATGGAGCGGAAAG-3', reverse, 5' TCCAGGCCCTGTAGCACTTG-3';
301 *Gapdh*: forward, 5'-CCATCTTCCAGGAGCGAGAC-3', reverse, 5'-GCCC
302 TTCCACAATGCCAAAG-3'. The thermal cycling conditions compromised of an initial
303 denaturation at 95°C for 3 minutes, followed by 35 cycles at 95°C for 30s, annealing
304 at 62°C for *Srpk1* or 58°C for *Gapdh* for 30s, 72°C for 1 min. This was followed by a
305 full extension at 72°C for 5 mins. PCR products were run on a 2% agarose gel with
306 25ng/ml ethidium bromide for 1hr 30 mins at 90V. The agarose gel was visualised on
307 a UV transilluminator GelDocEZ system. qRT-PCR was carried out for VEGF-A_{165}b
308 and VEGF-A_{165}a using isoform specific primers Forward:5'-
309 GGCAGCTTGAGTTAAACGAAC-3', Reverse: 5'-AGTCTTTCCTGGTGAGAGAT
310 CTGCA-3' as previously described [34]
311

312 **Statistical analysis.** Statistical analyses were completed on GraphPad Prism,
313 Microsoft Excel, FIJI and Laser Speckle imaging analysis software (Moor's
314 Instruments). All data is presented as the mean ± SEM as indicated in the figure
315 legends. In all cases $p<0.05$ was considered statistically significant.
316
317 **Results**
318 To determine the effect of SRPK1 inhibition on monocyte VEGF-A_{165}b we treated
319 monocytes from patients with PAD (N=9) with 3μM SPHINX31 (a selective SRPK1
320 inhibitor) overnight and measured VEGF-A_{165}a and VEGF-A_{165}b using isoform
321 specific ELISAs[35,15]. VEGF-A_{165}a expression was not detected in PAD monocytes,
322 but surprisingly was significantly increased by SRPK1 inhibition (Figure 1A). In
323 contrast, VEGF-A_{165}b expression was significantly reduced by SRPK1 inhibition
324 (Figure 1B). Monocytes from patients with dominance of VEGF-A_{165}b RNA as
325 measured by RT-PCR, were subjected to SPHINX31 treatment, which significantly
326 increased the ratio of VEGF-A_{165}a:VEGF-A_{165}b RNA as measured by qRT-PCR
327 (Figure 1C). To determine whether this change in expression would functionally
328 affect the ability of monocytes to induce angiogenesis we developed an in vitro
329 assay for VEGF-A_{165}b mediated inhibition of endothelial cell migration. Figure 1D
330 shows that in the presence of 1nM VEGF-A_{165}a, endothelial cell migration across a
331 transwell was significantly increased compared with control, but this was significantly
332 decreased by treatment with recombinant VEGF-A_{165}b. This inhibition was dose
333 dependently reversed with a neutralising antibody to VEGF-A_{165}b (Figure 1D). Figure
334 1D shows that culturing monocytes in the lower half of the transwell inhibits migration
335 towards VEGF-A_{165}a, and that this can be reversed by treatment with the neutralising
336 antibody to VEGF-A_{165}b. Figure 1E shows that treatment with an SRPK1 inhibitor
337 blocks the inhibition of migration by PAD monocytes. These results indicate that PAD
338 monocytes produce VEGF-A_{165}b, sufficiently to inhibit endothelial cell migration
339 towards 1nM VEGF-A_{165}a and that SRPK1 treatment switches splicing and
340 sufficiently to stop the inhibition of migration by VEGF-A_{165}b under these
341 circumstances. To determine whether this would be effective in vivo we used an
342 animal model of PAD previously shown to be VEGF-A_{165}b dependent[5].
343
344 **Impaired collateral revascularisation in Sfrp5 knockout (Sfrp5$^{-/-}$) mice is**
345 **reversed with SPHINX31, an SRPK1 inhibitor.**

346 Previous studies have identified that Sfrp5 acts to inhibit the non-canonical Wnt5a
347 signalling pathway in macrophages and impaired revascularisation in a hindlimb
348 ischemia model. This correlated with an upregulation of Wnt5a at a transcriptional
349 level in the ischemic limb[4,5], and upregulation of VEGF-A_{165}b in monocytes[5]. We
350 therefore used this model to determine whether SRPK1 was able to modulate the
351 angiogenic activity of monocytes in ischemia. Twenty Sfrp5$^{-/-}$ and twenty wild type
352 mice underwent left femoral artery ligation and the blood flow to the hind paws were
353 monitored non-invasively using laser speckle imaging on pre- and post-operative days
354 (Figure 2A). Quantitative analysis revealed that Sfrp5$^{-/-}$ had impaired revascularisation
355 compared to WT mice on days 21 (0.60 ± 0.04 vs 0.76 ± 0.04, p=0.007) and 28 (0.62
356 ± 0.04 vs 0.85 ± 0.08, p=0.0002) (Figure 2B). At the end of the study, in 4 sfrp5-/- and
357 3 wild types, gastrocgnemius muscle was taken and protein extracted. ELISA for
358 VEGF-A_{165}b demonstrated that the sfrp5$^{-/-}$ mice had significantly greater VEGF-A_{165}b
359 than the wild type (figure 2C) in both ischemic and contralateral muscle. The
360 gastrocnemius muscle was collected, sectioned, stained and imaged for arterioles and
361 capillaries (Figure 2D). The capillary density was unchanged in the ischemic
362 gastrocnemius muscle of both mouse groups (650.1 ± 43.7/mm^2 vs 721.9 ± 72.6/mm^2,
363 p=0.41) (Figure 2E). However, the arteriolar density was significantly reduced in the
364 ischemic gastrocnemius muscle of Sfrp5$^{-/-}$ mice (4.40 ± 0.90/mm^2) compared to WT
365 (7.01 ± 0.67/mm^2, p=0.04) (Figure 2F). To determine whether SRPK1 and SR protein
366 expression was altered in these mice, protein was extracted from total muscle tissue
367 and subjected to immunoblotting for SRSF1, SRSF6 and SRPK1. SRSF1 was
368 increased in both cytoplasm and nucleus of cells from muscle from Sfrp5$^{-/-}$ mice,
369 whereas SRSF6 was reduced. SRPK1 levels were increased in ischemia only in Sfrp5^{-}
370 $^{/-}$ mice (Supplementary Figure 1). To explore the significance of SRPK1 on
371 revascularisation, SPHINX31[24,36] was administered to Sfrp5$^{-/-}$ mice via an
372 intraperitoneal route after the ischemic hind limb surgery and bi-weekly thereafter.
373 Quantitative analysis of the speckle images (Figure 2G) revealed that the flow was
374 significantly increased in Sfrp5$^{-/-}$ treated with SPHINX31 on post-operative days 14
375 (0.55 ± 0.04 vs 0.93 ± 0.08, p=0.001) and days 21 (0.51 ± 0.05 vs 0.75 ± 0.07, p=0.04)
376 when compared to the Sfrp5$^{-/-}$ treated with DMSO alone (Figure 2H).
377
378 **Inhibition of SRPK1 improves revascularisation in LysM-Wnt5a^{GOF} mice.**

379 To determine whether SRPK1 inhibition would exert the same effect in a different
380 mouse model of Wnt5A activation, we used a monocytic Wnt5a overexpression
381 (LysM-Wnt5a^{GOF}) model. This resulted in a significant decrease in blood flow (Figure
382 3A) compared with wild type animals, which was reversed by SPHINX31 treatment.
383 Quantitative analysis of the speckle intensity revealed that the blood flow recovery was
384 significantly slower in LysM-Wnt5a^{GOF} mice when compared to WT mice on post-
385 operative day 3 (0.19 ± 0.03 vs 0.72 ± 0.09 compared with contralateral limb,
386 $p<0.0001$), 7 (0.40 ± 0.03 vs 0.82 ± 0.10, $p<0.0002$) and 14 (0.59 ± 0.08 vs 0.92 ±
387 0.05, $p=0.0039$) but this was completely reversed by treatment with SPHINX31 as
388 above (Figure 3B). Recovery between mouse groups was not different at post-
389 operative day 21, when gastrocnemius muscle was collected, stained and imaged for
390 capillary and arterioles (Figure 3C). The capillary density was significantly decreased
391 in the ischemic gastrocnemius muscle of LysM-Wnt5a^{GOF} (311 ± 18mm^2) when
392 compared with WT mice (491 ± 55mm^2, $p<0.05$) and SPHINX31 treated mice (516 ±
393 42.01/mm^2, $p<0.05$) (Figure 3D). Similarly, the arteriolar density was significantly
394 reduced in the ischemic gastrocnemius muscle of LysM-Wnt5a^{GOF} mice (4.32 ±
395 0.55/mm^2) compared to WT mice (19.22 ± 2.03/mm^2, $p=0.004$) and SPHINX31 treated
396 mice (20.45 ± 4.22/mm^2, $p=0.002$) (Figure 3E). This suggested that impaired
397 revascularisation of LysM-Wnt5a^{GOF} may be dependent on SRPK1.
398
399 **Monocytic-SRPK1 is responsible for impaired revascularisation in LysM-**
400 **Wnt5a^{GOF} mice.**
401 Systemic treatment with an SRPK1 inhibitor could have many effects on many tissues.
402 To determine whether monocytic-SRPK1 regulated the prolonged blood flow recovery
403 in LysM-Wnt5a^{GOF} mice, we generated a double transgenic, monocyte specific LysM
404 over-expressing, SRPK1 knockout mouse model (LysM-Wnt5a^{GOF}:SRPK1^{MoKO}).
405 Quantitative analysis of the speckle images revealed that revascularisation in LysM-
406 Wnt5a^{GOF} littermates had impaired flow compared to littermate control wild type mice
407 on post-operative days 3 (0.19 ± 0.03 vs 0.48 ± 0.07, $p=0.0034$) and 7 (0.40 ± 0.03 vs
408 0.68 ± 0.07, $p=0.004$), which was rescued on day 7 in LysM-Wnt5a^{GOF}:SRPK1^{MoKO}
409 mice (0.65 ± 0.08, $p=0.03$) (Figure 4A-B). There was a moderate, but not statistically
410 significant reduction in the capillary density in the ischemic gastrocnemius of LysM-
411 Wnt5a^{GOF} mice compared with wild type which was partially but not significantly
412 reversed by the SRPK1^{MOKO} (Figure 4C-D). However, the impaired arteriolar density

413 in the ischemic gastrocnemius muscle of LysM-Wnt5a^{GOF} mice (4.32 ± 0.55/mm^2) was
414 significantly reversed in the LysM-Wnt5a^{GOF}:SRPK1^{MoKO} mice (13.15 ± 2.48/mm^2,
415 p=0.007) and was comparable to WT mice (12.75 ± 1.60/mm^2, p=0.009) (Figure 4E).
416 Collectively, these results show that impaired revascularisation is dependent on
417 monocytic-SRPK1 in LysM-Wnt5a^{GOF} mice.
418
419 **SRPK1 knockout reverses impaired blood flow recovery in diet-induced obese**
420 **mice.**
421 Previous studies have confirmed that mice fed on a HF/HS diet have an increase in
422 Wnt5a expression in the ischemic gastrocnemius, which was co-localised to the
423 macrophages[5]. Therefore, we hypothesised that diet-induced obese mice would have
424 impaired blood flow recovery, which would be reversed with SRPK1^{MoKO}. Quantitative
425 analysis of the representative speckle images in Figure 5A revealed that the level of
426 the ischemia induced in the left hind limb of HF/HS-SRPK1^{MoKO} mice (0.12 ± 0.01) was
427 greater than that in HF/HS-WT mice (0.23 ± 0.03, p=0.02) (Figure 5B). Therefore, the
428 flow was normalised to post-operative day 0, which revealed that rate of
429 revascularisation was more rapid in obese-SRPK1^{MoKO} mice when compared to WT
430 mice on post-operative days 14 (5.21 ± 0.41 vs 3.29 ± 0.41, p=0.002), 21 (5.30 ± 0.40
431 vs 3.55 ± 0.41, p=0.003) and 28 (6.29 ± 0.51 vs 3.73 ± 0.46, p<0.0001) (Figure 5C).
432 Staining of capillaries and arterioles (Figure 5D) showed that HFHS-SRPK1^{MoKO} mice
433 had a higher capillary density and arteriolar density than HFHS wild type mice after
434 ischemia (Figure 5E).
435
436 **Discussion**
437 We show here that monocytes control VEGF splicing to be able to regulate
438 angiogenesis through SRPK1 using both transgenic models driving VEGF splicing to
439 the anti-angiogenic VEGF-A$_{165}$b isoform, pharmacological and genetic manipulation
440 of SRPK1 activity or expression, and human monocytes from patients with PAD. The
441 implications of the finding are consistently that SRPK1 inhibition switches monocytes
442 away from an anti-angiogenic phenotype, and in both the human monocyte ex vivo
443 assay and the mouse in vivo assay, this is sufficient to induce behaviours associated
444 with collateral formation (endothelial cell migration, new capillary and new arteriole
445 formation).

446 We show in human cells that monocytes, when co-cultured with endothelial
447 cells secrete the anti-angiogenic isoforms VEGF-A_{165}b, as shown by the use of a
448 neutralising antibody to VEGF-A_{165}b. This antibody is raised against the C-terminal tail
449 of VEGF-A_{165}b and is effective in detecting VEGF-A_{165}b and VEGF-A_{189}b and the
450 readthrough isoform VEGF-Ax[37]. We have previously shown that this antibody has
451 neutralising properties in the mouse models described here, which do not express
452 VEGF-Ax[5]. Treatment with SRPK1 inhibitor increased VEGF-A_{165}a from 0 to 40pg/ml,
453 and reduced VEGF-A_{165}b from 275 to 175pg/ml in the monocyte cell lysate.
454 Interestingly, monocytes secrete sufficient VEGF-A_{165}b to inhibit endothelial cell
455 migration, and the neutralising antibody to VEGF-A_{165}b completely reverses the
456 monocyte mediated inhibition. Given that these experiments include 1nM VEGF-A_{165}b,
457 we can assume that the concentrations of VEGF-A_{165}b in the media need to be close
458 to that to inhibit endothelial cell migration. The proportion of VEGF that is VEGF-A_{165}b
459 in the monocytes has changed from 100% to 80% with SRPK1 inhibition, but this is
460 sufficient to allow migration to occur. This suggest that the concentration of VEGF-
461 A_{165}b in the media must be close to the threshold for inhibition of VEGF-A_{165}a,
462 (potentially 1nM VEGF-A_{165}b:1nM VEGF-A_{165}a), and that switching the splicing
463 therefore switches that to 0.8nM VEGF-A_{165}b:1.2nM VEGF-A_{165}a, i.e. from 50% to
464 40% VEGF-A_{165}b. This again indicates that the switch in splicing does not have to be
465 very great to allow angiogenesis to happen. Given that the angiogenic drive in the
466 ischemic tissue is from the hypoxic muscle the balance between VEGF-A_{165}b and
467 VEGF-A_{165}a in the tissues is likely to be critical for the efficacy of a splicing switch.
468 There have been surprisingly few studies investigating the effect of monocytes on
469 endothelial cells in transwell studies (removing the interfering effects of contact
470 between the cells). It has previously been shown that monocytes from healthy
471 individuals stimulated to differentiate into macrophages can produce angiogenic
472 effects by production of VEGF-A, depending on the differentiation state[38] and that this
473 is inhibited by treatment with IL4 as this enhances production of the inhibitory isoform
474 of VEGFR1, soluble flt1[39]. This suggests that control of splicing of angiogenic
475 processes in monocytes is a process that depends on the differentiation state of the
476 monocytes and the environment in which they find themselves.
477 We also show that in transgenic animals with enhanced Wnt5a monocyte signalling[5],
478 and in animals in which this signalling is induced metabolically[4], and in which VEGF-
479 A_{165}b is upregulated in monocytes[5], there is impaired collateral formation, which is

480 reversed by SRPK1 inhibition. This finding is in direct contrast to the well described
481 (including by us) action of SRPK1 inhibition in many other cell types, and was highly
482 surprising, as we have previously shown that SRPK1 inhibition switches splicing from
483 the VEGF-A_{165}a isoform to the VEGF-A_{165}b in epithelial cells (retinal pigmented
484 epithelial cells[33], glomerular visceral epithelial cells[27], in neurons (dorsal root ganglion
485 neurons[40], and SHSY5Y neurons[41]), and in cancer cells (melanoma[42], prostate cancer
486 [31] and cholangiocarcinoma cells[43], and others have shown it regulates VEGF splicing
487 in renal carcinoma[44], melanoma and Hela cells[45] and lung alveolar epithelial cells[46].
488 Thus it appears that the control of VEGF splicing is not fixed, but dependent on either
489 cell type or cell environment. While we cannot say for certain which of these is
490 deterministic, it is unlikely that the diabetic environment controls whether SRPK1
491 determines splicing to VEGF-A_{165}b or VEGF-A_{165}a as SRPK1 inhibition switches
492 splicing to VEGF-A_{165}b in diabetic retinal epithelial cells[30], but the data here suggests
493 that it switches it to VEGF-A_{165}a in diabetic monocytes. SRPK1 acts via
494 phosphorylation of SR rich sequences in SR proteins such as SRSF1[47]. While we have
495 shown that SRSF1 is the key target for SRPK1 in epithelial cells, we have not shown
496 that for monocytes, and it should be noted that SRSF2 has been implicated in control
497 of VEGF splicing in lung cancer cells[48] and in monocytes[5], suggesting that potentially
498 SRPK1 may act in monocytes by phosphorylation of SRSF2 or other SRSF proteins.
499 Furthermore, SRSF1 and SRPK1 are both significantly upregulated in ischemic Sfrp5^{-}
500 $^{/-}$ mice (Supp Figure 1), strongly suggesting that in monocytes, Wnt5a signalling can
501 change splicing factor protein expression and hence alter the role of SR protein kinase.
502 Finally, we describe here for the first time a viable SRPK1 inducible knockout
503 mouse. Previously, Wang et al have described a conditional SRPK1 with a deletion of
504 exon 3 this mouse line was lost early after its development, and no further information
505 has been available[49]. We made numerous attempts to recreate this line using exon 3
506 and exon 1 Lox-P flanking, but this was unsuccessful, presumably due to disruption of
507 regulatory element within the introns. The insertion of the LoxP sites flanking exon 7
508 however, resulted in a robust knockout when crossed with Cre Driver lines, and the
509 parental line has a normal phenotype. According to the International Mouse Strain
510 Resource, there are 44 strains of mice that have been generated as ES cells that have
511 a gene trap, one that is a CRISPR-Cas9 exon 3 knockout, and one that has a loxP
512 exon 3 flanking region. However, these mice have never been published or validated.

While we have driven the knockout here in monocytes by crossing the SRPK1-LoxP mouse with a monocyte specific driver line, it is clearly of interest to generate lines where SRPK1 is knocked out in tissues in which VEGF expression is controlled in the opposite direction, e.g. in retinal epithelial cells[33], retinal neurons[30], and in renal epithelial cells[27], and determine whether control of isoform expression can affect diabetic nephropathy or retinopathy. SRPK1 knockout has been shown to be embryonically lethal before e14.5, as it appears to affect heart development[49] so this mouse is an ideal tool to investigate the role of SRPK1 in adult physiology. Further work will show how tissue specific and development stage specific SRPK1 knockout affects tissue function, and also the effects of global SRPK1 knockout in adult tissues. It was of interest that the monocyte specific knockout of SRPK1 (which would have occurred in the myeloid lineage from birth onwards[50]) had impaired flow after ligation indicating that residual collateral formation during development was impaired in these mice suggesting that monocytic SRPK1 is involved in the development of blood vessels.

In summary we show here that splicing control is cell type dependent, that monocytic SRPK1 controls VEGF splicing and that targeting SRPK1 can enhance collateral formation in models of peripheral vascular disease

Acknowledgements.

This work was funded by the MRC (MR/K020366/1, MR/K013157/1), The British Heart Foundation (PG/21/10796, PG/13/47/30337, TG/18/3/33773) and the BBSRC Doctoral Training Program (BB/M008770/1).

References

1. Abaci A, Oguzhan A, Kahraman S, Eryol NK, Unal S, Arinc H, Ergin A. Effect of diabetes mellitus on formation of coronary collateral vessels. *Circulation*. 1999;99:2239-2242.
2. Yadav SS, Hussain S, Dwivedi P, Khattri S, Sawlani KK, Usman K. Assesement of serum Sfrp5/Wnt-5a level and its utility in the risk stratification of treatment naive patients with metabolic syndrome. *J Immunoassay Immunochem*. 2023;44:1-12. doi: 10.1080/15321819.2022.2104125
3. Murdoch CE, Shuler M, Haeussler DJ, Kikuchi R, Bearelly P, Han J, Watanabe Y, Fuster JJ, Walsh K, Ho YS, et al. Glutaredoxin-1 up-regulation induces soluble vascular endothelial growth factor receptor 1, attenuating post-ischemia limb revascularization. *J Biol Chem*. 2014;289:8633-8644. doi: 10.1074/jbc.M113.517219

549 4. Ouchi N, Higuchi A, Ohashi K, Oshima Y, Gokce N, Shibata R, Akasaki Y, Shimono A,
550 Walsh K. Sfrp5 is an anti-inflammatory adipokine that modulates metabolic
551 dysfunction in obesity. *Science*. 2010;329:454-457. doi: science.1188280 [pii]
552 10.1126/science.1188280
553 5. Kikuchi R, Nakamura K, MacLauchlan S, Ngo DT, Shimizu I, Fuster JJ, Katanasaka Y,
554 Yoshida S, Qiu Y, Yamaguchi TP, et al. An antiangiogenic isoform of VEGF-A
555 contributes to impaired vascularization in peripheral artery disease. *Nat Med*.
556 2014;20:1464-1471. doi: 10.1038/nm.3703
557 6. Lolmede K, Duffaut C, Zakaroff-Girard A, Bouloumie A. Immune cells in adipose
558 tissue: key players in metabolic disorders. *Diabetes Metab*. 2011;37:283-290. doi:
559 S1262-3636(11)00061-9 [pii]
560 10.1016/j.diabet.2011.03.002
561 7. Panutsopulos D, Zafiropoulos A, Krambovitis E, Kochiadakis GE, Igoumenidis NE,
562 Spandidos DA. Peripheral monocytes from diabetic patients with coronary artery
563 disease display increased bFGF and VEGF mRNA expression. *J Transl Med*. 2003;1:6.
564 doi: 10.1186/1479-5876-1-6
565 1479-5876-1-6 [pii]
566 8. Tchaikovski V, Olieslagers S, Bohmer FD, Waltenberger J. Diabetes mellitus activates
567 signal transduction pathways resulting in vascular endothelial growth factor
568 resistance of human monocytes. *Circulation*. 2009;120:150-159. doi:
569 CIRCULATIONAHA.108.817528 [pii]
570 10.1161/CIRCULATIONAHA.108.817528
571 9. Hu W, Li L, Yang M, Luo X, Ran W, Liu D, Xiong Z, Liu H, Yang G. Circulating Sfrp5 is a
572 signature of obesity-related metabolic disorders and is regulated by glucose and
573 liraglutide in humans. *J Clin Endocrinol Metab*. 2013;98:290-298. doi: jc.2012-2466
574 [pii]
575 10.1210/jc.2012-2466
576 10. Hu Z, Deng H, Qu H. Plasma SFRP5 levels are decreased in Chinese subjects with
577 obesity and type 2 diabetes and negatively correlated with parameters of insulin
578 resistance. *Diabetes Res Clin Pract*. 2013. doi: S0168-8227(12)00491-3 [pii]
579 10.1016/j.diabres.2012.11.026
580 11. Harper SJ, Bates DO. VEGF-A splicing: the key to anti-angiogenic therapeutics? *Nat*
581 *Rev Cancer*. 2008;8:880-887.
582 12. Bates DO, Cui TG, Doughty JM, Winkler M, Sugiono M, Shields JD, Peat D, Gillatt D,
583 Harper SJ. VEGF165b, an inhibitory splice variant of vascular endothelial growth
584 factor, is down-regulated in renal cell carcinoma. *Cancer Res*. 2002;62:4123-4131.
585 13. Kawamura H, Li X, Harper SJ, Bates DO, Claesson-Welsh L. Vascular endothelial
586 growth factor (VEGF)-A165b is a weak in vitro agonist for VEGF receptor-2 due to
587 lack of coreceptor binding and deficient regulation of kinase activity. *Cancer Res*.
588 2008;68:4683-4692.
589 14. Cebe Suarez S, Pieren M, Cariolato L, Arn S, Hoffmann U, Bogucki A, Manlius C, Wood
590 J, Ballmer-Hofer K. A VEGF-A splice variant defective for heparan sulfate and
591 neuropilin-1 binding shows attenuated signaling through VEGFR-2. *Cell Mol Life Sci*.
592 2006;63:2067-2077.
593 15. Woolard J, Wang WY, Bevan HS, Qiu Y, Morbidelli L, Pritchard-Jones RO, Cui TG,
594 Sugiono M, Waine E, Perrin R, et al. VEGF165b, an inhibitory vascular endothelial

growth factor splice variant: mechanism of action, in vivo effect on angiogenesis and endogenous protein expression. *Cancer Res*. 2004;64:7822-7835.

16. Bevan HS, van den Akker NM, Qiu Y, Polman JA, Foster RR, Yem J, Nishikawa A, Satchell SC, Harper SJ, Gittenberger-de Groot AC, et al. The alternatively spliced anti-angiogenic family of VEGF isoforms VEGFxxxb in human kidney development. *Nephron Physiol*. 2008;110:p57-67.
17. Magnussen AL, Rennel ES, Hua J, Bevan HS, Beazley Long N, Lehrling C, Gammons M, Floege J, Harper SJ, Agostini HT, et al. VEGF-A165b is cytoprotective and antiangiogenic in the retina. *Invest Ophthalmol Vis Sci*. 2010;51:4273-4281. doi: iovs.09-4296 [pii]
10.1167/iovs.09-4296
18. Peach CJ, Kilpatrick LE, Friedman-Ohana R, Zimmerman K, Robers MB, Wood KV, Woolard J, Hill SJ. Real-Time Ligand Binding of Fluorescent VEGF-A Isoforms that Discriminate between VEGFR2 and NRP1 in Living Cells. *Cell Chem Biol*. 2018;25:1208-1218 e1205. doi: 10.1016/j.chembiol.2018.06.012
19. Ganta VC, Choi M, Kutateladze A, Annex BH. VEGF165b Modulates Endothelial VEGFR1-STAT3 Signaling Pathway and Angiogenesis in Human and Experimental Peripheral Arterial Disease. *Circ Res*. 2017;120:282-295. doi: 10.1161/CIRCRESAHA.116.309516
20. Ganta VC, Choi M, Farber CR, Annex BH. Antiangiogenic VEGF165b Regulates Macrophage Polarization via S100A8/S100A9 in Peripheral Artery Disease. *Circulation*. 2019;139:226-242. doi: 10.1161/CIRCULATIONAHA.118.034165
21. Kuppuswamy S, Annex BH, Ganta VC. Targeting Anti-Angiogenic VEGF165b-VEGFR1 Signaling Promotes Nitric Oxide Independent Therapeutic Angiogenesis in Preclinical Peripheral Artery Disease Models. *Cells*. 2022;11. doi: 10.3390/cells11172676
22. Rios-Navarro C, Hueso L, Diaz A, Marcos-Garces V, Bonanad C, Ruiz-Sauri A, Vila JM, Sanz MJ, Chorro FJ, Piqueras L, et al. Role of antiangiogenic VEGF-A165b in angiogenesis and systolic function after reperfused myocardial infarction. *Rev Esp Cardiol (Engl Ed)*. 2020. doi: 10.1016/j.rec.2020.03.013
23. Hueso L, Rios-Navarro C, Ruiz-Sauri A, Chorro FJ, Nunez J, Sanz MJ, Bodi V, Piqueras L. Dynamics and implications of circulating anti-angiogenic VEGF-A165b isoform in patients with ST-elevation myocardial infarction. *Scientific reports*. 2017;7:9962. doi: 10.1038/s41598-017-10505-9
24. Batson J, Toop HD, Redondo C, Babaei-Jadidi R, Chaikuad A, Wearmouth SF, Gibbons B, Allen C, Tallant C, Zhang J, et al. Development of Potent, Selective SRPK1 Inhibitors as Potential Topical Therapeutics for Neovascular Eye Disease. *ACS chemical biology*. 2017;12:825-832. doi: 10.1021/acschembio.6b01048
25. Muraki M, Ohkawara B, Hosoya T, Onogi H, Koizumi J, Koizumi T, Sumi K, Yomoda J, Murray MV, Kimura H, et al. Manipulation of alternative splicing by a newly developed inhibitor of Clks. *J Biol Chem*. 2004;279:24246-24254.
26. Nowak DG, Woolard J, Amin EM, Konopatskaya O, Saleem MA, Churchill AJ, Ladomery MR, Harper SJ, Bates DO. Expression of pro- and anti-angiogenic isoforms of VEGF is differentially regulated by splicing and growth factors. *J Cell Sci*. 2008;121:3487-3495. doi: 10.1242/jcs.016410
27. Amin EM, Oltean S, Hua J, Gammons MV, Hamdollah-Zadeh M, Welsh GI, Cheung MK, Ni L, Kase S, Rennel ES, et al. WT1 mutants reveal SRPK1 to be a downstream

641 angiogenesis target by altering VEGF splicing. *Cancer Cell*. 2011;20:768-780. doi:
642 10.1016/j.ccr.2011.10.016
643 28. Nowak DG, Amin EM, Rennel ES, Hoareau-Aveilla C, Gammons M, Damodoran G,
644 Hagiwara M, Harper SJ, Woolard J, Ladomery MR, et al. Regulation of vascular
645 endothelial growth factor (VEGF) splicing from pro-angiogenic to anti-angiogenic
646 isoforms: a novel therapeutic strategy for angiogenesis. *J Biol Chem*. 2010;285:5532-
647 5540. doi: M109.074930 [pii]
648 10.1074/jbc.M109.074930
649 29. Merdzhanova G, Gout S, Keramidas M, Edmond V, Coll JL, Brambilla C, Brambilla E,
650 Gazzeri S, Eymin B. The transcription factor E2F1 and the SR protein SC35 control the
651 ratio of pro-angiogenic versus antiangiogenic isoforms of vascular endothelial
652 growth factor-A to inhibit neovascularization in vivo. *Oncogene*. 2010;29:5392-5403.
653 doi: onc2010281 [pii]
654 10.1038/onc.2010.281
655 30. Malhi NK, Allen CL, Stewart E, Horton KL, Riu F, Batson J, Amoaku W, Morris JC, Arkill
656 KP, Bates DO. Serine-arginine-rich protein kinase-1 inhibition for the treatment of
657 diabetic retinopathy. *Am J Physiol Heart & Circ* 2022;322:H1014-H1027. doi:
658 10.1152/ajpheart.00001.2022
659 31. Mavrou A, Brakspear K, Hamdollah-Zadeh M, Damodaran G, Babaei-Jadidi R, Oxley J,
660 Gillatt DA, Ladomery MR, Harper SJ, Bates DO, et al. Serine-arginine protein kinase 1
661 (SRPK1) inhibition as a potential novel targeted therapeutic strategy in prostate
662 cancer. *Oncogene*. 2015;34:4311-4319. doi: 10.1038/onc.2014.360
663 32. Gammons MV, Dick AD, Harper SJ, Bates DO. SRPK1 Inhibition Modulates VEGF
664 Splicing to Reduce Pathological Neovascularization in a Rat Model of Retinopathy of
665 Prematurity. *Invest Ophthalmol Vis Sci*. 2013;54:5797-5806. doi: 10.1167/iovs.13-
666 11634
667 33. Gammons MV, Fedorov O, Ivison D, Du C, Clark T, Hopkins C, Hagiwara M, Dick AD,
668 Cox R, Harper SJ, et al. Topical Antiangiogenic SRPK1 Inhibitors Reduce Choroidal
669 Neovascularization in Rodent Models of Exudative AMD. *Invest Ophthalmol Vis Sci*.
670 2013;54:6052-6062. doi: 10.1167/iovs.13-12422
671 34. Bates DO, Mavrou A, Qiu Y, Carter JG, Hamdollah-Zadeh M, Barratt S, Gammons MV,
672 Millar AB, Salmon AH, Oltean S, et al. Detection of VEGF-A(xxx)b isoforms in human
673 tissues. *PLoS One*. 2013;8:e68399. doi: 10.1371/journal.pone.0068399
674 35. Alalwany R, Hawtrey T, Morgan K, Morris JC, Donaldson LF, Bates DO. Vascular
675 endothelial growth factor isoforms differentially protect neurons against neurotoxic
676 events associated with Alzheimer's disease. *Frontiers in Molecular Neuroscience*.
677 2023;in press.
678 36. Tzelepis K, De Braekeleer E, Aspris D, Barbieri I, Vijayabaskar MS, Liu WH, Gozdecka
679 M, Metzakopian E, Toop HD, Dudek M, et al. SRPK1 maintains acute myeloid
680 leukemia through effects on isoform usage of epigenetic regulators including BRD4.
681 *Nature communications*. 2018;9:5378. doi: 10.1038/s41467-018-07620-0
682 37. Eswarappa SM, Potdar AA, Koch WJ, Fan Y, Vasu K, Lindner D, Willard B, Graham LM,
683 DiCorleto PE, Fox PL. Programmed Translational Readthrough Generates
684 Antiangiogenic VEGF-Ax. *Cell*. 2014;157:1605-1618. doi: 10.1016/j.cell.2014.04.033
685 38. Wu WK, Llewellyn OP, Bates DO, Nicholson LB, Dick AD. IL-10 regulation of
686 macrophage VEGF production is dependent on macrophage polarisation and
687 hypoxia. *Immunobiology*. 2010;215:796-803. doi: 10.1016/j.imbio.2010.05.025

39. Wu WK, Georgiadis A, Copland DA, Liyanage S, Luhmann UF, Robbie SJ, Liu J, Wu J, Bainbridge JW, Bates DO, et al. IL-4 regulates specific Arg-1(+) macrophage sFlt-1-mediated inhibition of angiogenesis. *Am J Pathol*. 2015;185:2324-2335. doi: 10.1016/j.ajpath.2015.04.013
40. Hulse RP, Beazley-Long N, Hua J, Kennedy H, Prager J, Bevan H, Qiu Y, Fernandes ES, Gammons MV, Ballmer-Hofer K, et al. Regulation of alternative VEGF-A mRNA splicing is a therapeutic target for analgesia. *Neurobiology of disease*. 2014;71:245-259. doi: 10.1016/j.nbd.2014.08.012
41. Alalwany RH, Hawtrey T, Morgan K, Morris JC, Donaldson LF, Bates DO. Vascular endothelial growth factor isoforms differentially protect neurons against neurotoxic events associated with Alzheimer's disease. *Front Mol Neurosci*. 2023;16:1181626. doi: 10.3389/fnmol.2023.1181626
42. Gammons MV, Lucas R, Dean R, Coupland SE, Oltean S, Bates DO. Targeting SRPK1 to control VEGF-mediated tumour angiogenesis in metastatic melanoma. *Br J Cancer*. 2014;111:477-485. doi: 10.1038/bjc.2014.342
43. Supradit K, Boonsri B, Duangdara J, Thitiphatphuvanon T, Suriyonplengsaeng C, Kangsamaksin T, Janvilisri T, Tohtong R, Yacqub-Usman K, Grabowska AM, et al. Inhibition of serine/arginine-rich protein kinase-1 (SRPK1) prevents cholangiocarcinoma cells induced angiogenesis. *Toxicol In Vitro*. 2022;82:105385. doi: 10.1016/j.tiv.2022.105385
44. Pan XW, Xu D, Chen WJ, Chen JX, Chen WJ, Ye JQ, Gan SS, Zhou W, Song X, Shi L, et al. USP39 promotes malignant proliferation and angiogenesis of renal cell carcinoma by inhibiting VEGF-A(165b) alternative splicing via regulating SRSF1 and SRPK1. *Cancer Cell Int*. 2021;21:486. doi: 10.1186/s12935-021-02161-x
45. Li Q, Zeng C, Liu H, Yung KWY, Chen C, Xie Q, Zhang Y, Wan SWC, Mak BSW, Xia J, et al. Protein-Protein Interaction Inhibitor of SRPKs Alters the Splicing Isoforms of VEGF and Inhibits Angiogenesis. *iScience*. 2021;24:102423. doi: 10.1016/j.isci.2021.102423
46. Wagner KD, El Mai M, Ladomery M, Belali T, Leccia N, Michiels JF, Wagner N. Altered VEGF Splicing Isoform Balance in Tumor Endothelium Involves Activation of Splicing Factors Srpk1 and Srsf1 by the Wilms' Tumor Suppressor Wt1. *Cells*. 2019;8. doi: 10.3390/cells8010041
47. Ghosh G, Adams JA. Phosphorylation mechanism and structure of serine-arginine protein kinases. *FEBS J*. 2011;278:587-597. doi: 10.1111/j.1742-4658.2010.07992.x
48. Gout S, Brambilla E, Boudria A, Drissi R, Lantuejoul S, Gazzeri S, Eymin B. Abnormal expression of the pre-mRNA splicing regulators SRSF1, SRSF2, SRPK1 and SRPK2 in non small cell lung carcinoma. *PLoS One*. 2012;7:e46539. doi: 10.1371/journal.pone.0046539
49. Wang P, Zhou Z, Hu A, Ponte de Albuquerque C, Zhou Y, Hong L, Sierecki E, Ajiro M, Kruhlak M, Harris C, et al. Both decreased and increased SRPK1 levels promote cancer by interfering with PHLPP-mediated dephosphorylation of Akt. *Mol Cell*. 2014;54:378-391. doi: 10.1016/j.molcel.2014.03.007
50. Clausen BE, Burkhardt C, Reith W, Renkawitz R, Forster I. Conditional gene targeting in macrophages and granulocytes using LysMcre mice. *Transgenic Res*. 1999;8:265-277. doi: 10.1023/a:1008942828960

734

735 **Figure Legends**

736 **Figure 1. SRPK1 inhibition switches splicing to the angiogenic forms of VEGF**
737 **in PAD monocytes. (A).** Monocytes from patients with PAD were cultured for 24
738 hours in the presence of 3μM of SRPK1 inhibitor SPHINX31 or vehicle (0.1%
739 DMSO). Protein was extracted and (A) VEGF-A_{165}a or (B) VEGF-A_{165}b measured by
740 isoform specific ELISA. (C) RNA was extracted from monocytes incubated with
741 either vehicle or SPHINX31 and VEGF-A_{165}b and VEGF-A_{165}a measured by qRT-
742 PCR. (D) Endothelial cells seeded onto the upper side of a transwell membrane and
743 cultured with either media (0.1% serum control), 1nM VEGF-A_{165}a, or 1nM VEGF-
744 A_{165}a and monocytes from PAD patients with increasing concentration of anti-VEGF-
745 A_{165}b antibody in the lower half of the transwell. After 12 hours the number of
746 endothelial cells that had migrated were calculated. E). Endothelial cell migration in
747 response to monocytes treated with 3μM SPHINX31.

748

749 **Figure 2. SRPK1 inhibition with SPHINX31 reverses impaired revascularisation**
750 **in Sfrp5$^{-/-}$ mice. (A)** WT and Sfrp5$^{-/-}$ mice underwent left femoral artery ligation and
751 the blood flow to the paw was quantified using the laser speckle imaging system, as
752 shown in the representative speckle images. **(B)** Measurement of VEGF-A_{165}b from
753 muscle tissue from sfrp5$^{-/-}$ and wild type mice. Sfrp5$^{-/-}$ mice (N=4) had significantly
754 greater VEGF-A_{165}b expression than the wild type controls (N=3) in both ischemic and
755 contralateral muscle. **(C)** Quantitative analysis of the ischemic/ non-ischemic speckle
756 intensity was calculated through to post-operative day 28**.** Results are shown as the
757 mean ± SEM (N=19-20/group). Data was analysing using a two-way ANOVA with
758 post-hoc Bonferroni's test. **(D)** Confocal images from the representative muscle
759 sections of the gastrocnemius on post-operative day 28 stained with isolectin B4 for
760 endothelial (green) and α-smooth muscle actin for vascular smooth muscle cells (red).
761 **(E)** Capillary density was not changed in WT and Sfrp5$^{-/-}$ mice. **(F)** Arteriole density is
762 reduced in Sfrp5$^{-/-}$ mice when compared to WT mice. Results are shown as the mean
763 ± SEM (N=8/group). Data was analysing using an unpaired t-test. **(G)** Sfrp5$^{-/-}$ mice
764 received an intraperitoneal dose of DMSO or SPHINX31 (0.8mg/kg) bi-weekly for the
765 duration of the study. The representative speckle images are shown on pre-operative
766 day and on post-operative days 3, 7, 14, 21 and 28. **(H)** Quantitative analysis of the

767 ischemic/ non-ischemic speckle intensity was calculated through to post-operative day
768 28**.** Results are shown as the mean ± SEM (N=8-14/group). Data was analysed using
769 a two-way ANOVA with post-hoc Bonferroni's test. *p<0.05, **p<0.01, ***p<0.001.
770
771
772 **Figure 3. SRPK1 inhibition improves (and does not further impair) the blood flow**
773 **recovery in LysM-Wnt5a^{GOF} mice. (A)** LysM-Wnt5a^{GOF} mice underwent left femoral
774 artery ligation followed by treatment with SPHINX31 biweekly (0.8mg/kg, i.p) or vehicle
775 for the duration of the study. Blood flow to the paw was quantified using the laser
776 speckle imaging system, as shown in the representative speckle images. **(B)**
777 Quantitative analysis of the ischemic/ non-ischemic speckle intensity was calculated
778 through to post-operative day 21**.** Results are shown as the mean ± SEM (N=7-
779 9/group). Data was analysed using a two-way ANOVA with post-hoc Bonferroni's test.
780 **(C)** Confocal images from the representative muscle sections of the gastrocnemius on
781 post-operative day 21 stained with isolectin B4 for endothelial (green) and a-smooth
782 muscle actin for vascular smooth muscle cells (red). **(D)** The capillary density was
783 increased in LysM-Wnt5a^{GOF} treated with SPHINX31 compared with LysM-Wnt5a^{GOF}
784 mice and matched the density in WT mice. **(E)** The arteriole density was increased in
785 LysM-Wnt5a^{GOF} treated with SPHINX31 compared with LysM-Wnt5a^{GOF} mice and
786 matched the density in WT mice. Results are shown as the mean ± SEM (N=4-
787 5/group). Data was analysing using a one-way ANOVA with post hoc Bonferroni's test.
788 *p<0.05, **p<0.01, ***p<0.001, ****p<0.0001.
789
790 **Figure 5. Impaired revascularisation in LysM-Wnt5a^{GOF} mice is controlled by**
791 **monocyte specific SRPK1 activity *in vivo*. (A)** WT, LysM-Wnt5a^{GOF} and LysM-
792 Wnt5aGOF: SRPK1^{MoKO} mice underwent left femoral artery ligation Blood flow to the
793 paw was quantified using the laser speckle imaging system, as shown in the
794 representative speckle images. **(B)** Quantitative analysis of the ischemic/ non-
795 ischemic speckle intensity was calculated through to post-operative day 21**.** Results
796 are shown as the mean ± SEM (N=7-14/group). Data was analysed using a two-way
797 ANOVA with post-hoc Bonferroni's test. **(C)** Confocal images from the representative
798 muscle sections of the gastrocnemius muscle on post-operative day 21 stained with
799 isolectin B4 for endothelial (green) and a-smooth muscle actin for vascular smooth
800 muscle cells (red). **(D)** The capillary density in WT, LysM-Wnt5a^{GOF} and LysM-

801 Wnt5aGOF: SRPK1^{MoKO} mice was the same on post-operative day 21. **(E)** The
802 arteriole density was increased in LysM-Wnt5a^{GOF}: SRPK1^{MoKO} mice compared with
803 LysM-Wnt5a^{GOF} mice and matched the density in WT mice. Results are shown as the
804 mean ± SEM (N=4-5/group). Data was analysing using a one-way ANOVA with post
805 hoc Bonferroni's test. *p<0.05, **p<0.01, ***p<0.001, ****p<0.0001.
806
807 **Figure 6. Blood flow recovery is reversed in SRPK1^{MoKO} mice fed on a HF/HS**
808 **diet. (A)** WT and SRPK1^{MoKO} mice were fed on a HF/HS diet underwent left femoral
809 artery ligation Blood flow to the paw was quantified using the laser speckle imaging
810 system, as shown in the representative speckle images. **(B) (C)** Quantitative analysis
811 of the ischemic/ non-ischemic speckle intensity was calculated through to post-
812 operative day 28. **(B)** The level of ischemia induced on post-operative day 0 was
813 greater in SRPK1^{MoKO} mice compared to WT. Results are shown as the mean ± SEM
814 (N=9-11/group). Data was analysed using an unpaired t-test. **(C)** Data was further
815 normalised to post-operative day 0 of each respective mouse in each group through
816 to post-operative day 28. Results indicate the mean ± SEM (N=9-11/group). **(D)** The
817 capillary density in ischemic muscle of SRPK1^{MoKO} mice was significantly greater than
818 wild type controls in obese animals. **(E)** The arteriole density in obese mice was
819 increased in ischemic muscle of SRPK1^{MoKO} mice compared with wild type controls
820 (N=4-5/group). Data was analysing using a one-way ANOVA with post hoc
821 Bonferroni's test. *p<0.05, **p<0.01, ***p<0.001, ****p<0.0001.Data was analysed
822 using a two-way ANOVA with post hoc Bonferroni test. *p<0.05, **p<0.01,
823 ****p<0.0001.
824
825
826 **Supplementary Figure 1.** Muscle tissue was taken from Sfrp5$^{-/-}$ or wild type
827 littermate mice 7 days after ischemia was induced in the left hind limb. Cells were
828 disaggregated and nuclear extract made and both nuclear and cytoplasmic extract
829 subjected to immunoblotting for SRSF1 and SRSF6. Whole protein extract was
830 subjected to immunoblotting for SRPK1.
831
832 **Supplementary Figure 2**. **(A).** Generation of the SRPK1 conditional knockout.
833 Homologues recombination was used to insert LoxP sites either side of exon 7 of
834 SRPK1. This results in deletion of exon 7 and loss of SRPK1 RNA presumably due
835 to nonsense mediated decay. **(B)** CD11b^{+} Monocytes were extracted from mouse
836 spleens and bone marrow from LysM-Cre:SRPK1$^{loxp/loxp}$ mice (SRPK1^{MOKO})or wild
837 type littermates (Cre negative mice) and subjected to PCR for SRPK1. In wild type

838 mice SRPK1 was expressed in CD11b^{+} and CD11b^{-} cells from both bone marrow
839 and spleen, but was only expressed in CD11^{-}cells from spleen in the SRPK1^{MOKO}.

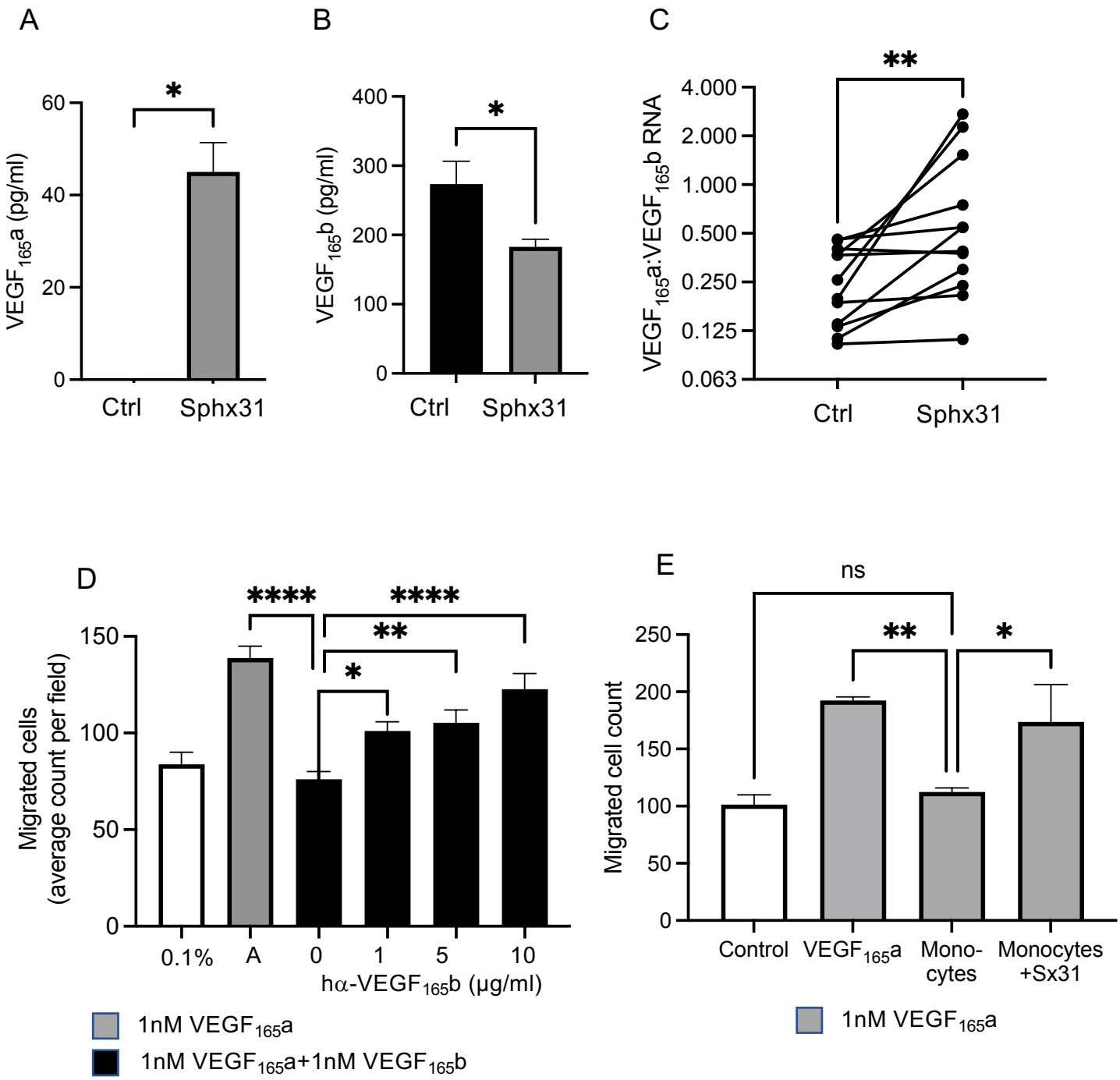
A
B
C
D
E
VEGF165a (pg/ml)
VEGF165b (pg/ml)
VEGF165a:VEGF165b RNA
Ctrl
Sphx31
Migrated cells
(average count per field)
0.1%
A
0
1
5
10
hα-VEGF165b (µg/ml)
1nM VEGF165a
1nM VEGF165a+1nM VEGF165b
ns
Migrated cell count
Control
VEGF165a
Mono-
cytes
Monocytes
+Sx31
1nM VEGF165a

Figure 1

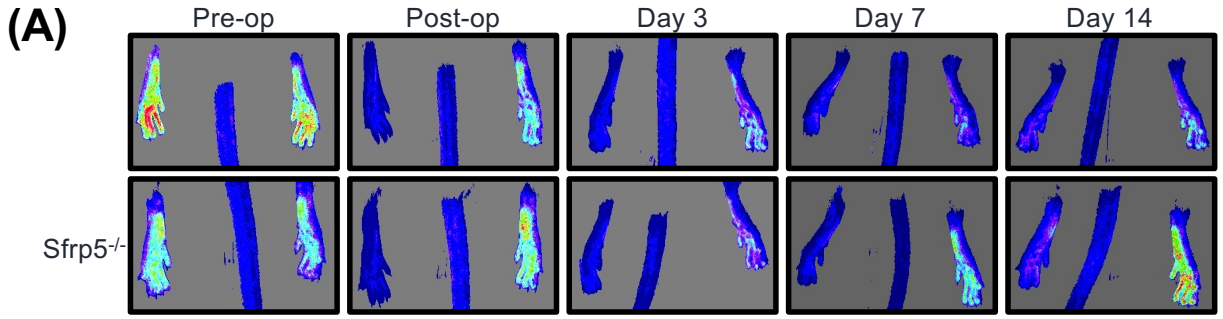
(A)
Pre-op
Post-op
Day 3
Day 7
Day 14
Sfrp5-/-

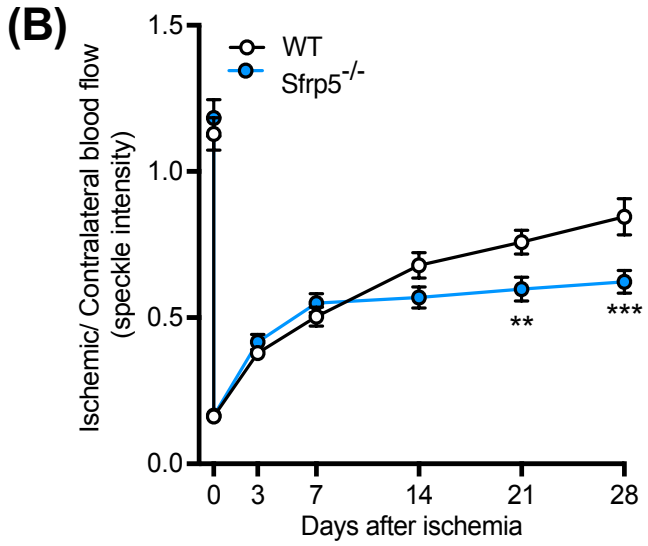
(B)
WT
Sfrp5-/-
Ischemic/ Contralateral blood flow (speckle intensity)
1.5
1.0
0.5
0.0
0
3
7
14
21
28
Days after ischemia
**
***

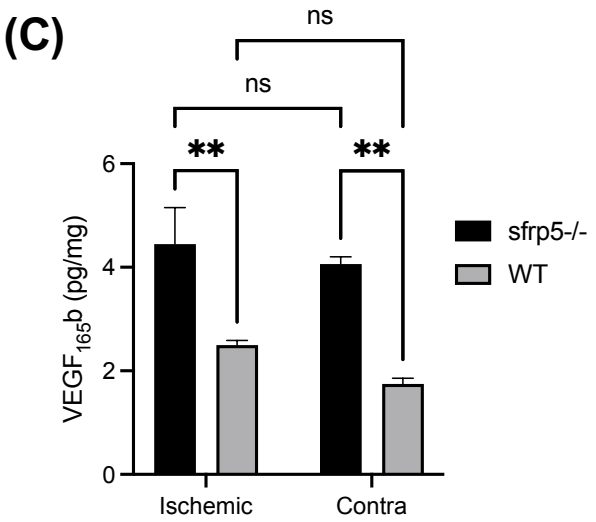
(C)
ns
ns
**
**
VEGF165b (pg/mg)
6
4
2
0
Ischemic
Contra
sfrp5-/-
WT

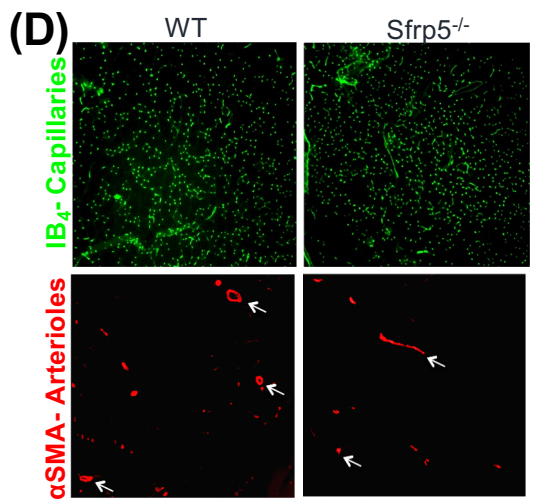
(D)
WT
Sfrp5-/-
IB4- Capillaries
αSMA- Arterioles

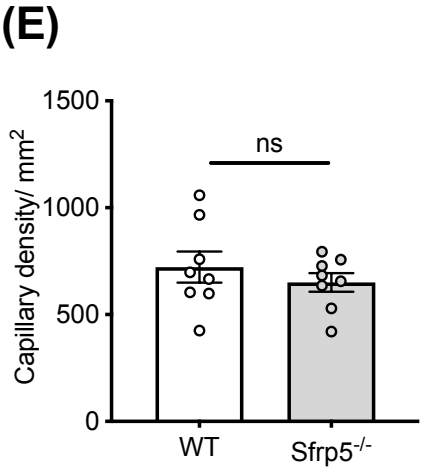
(E)
Capillary density/ mm2
1500
1000
500
0
ns
WT
Sfrp5-/-

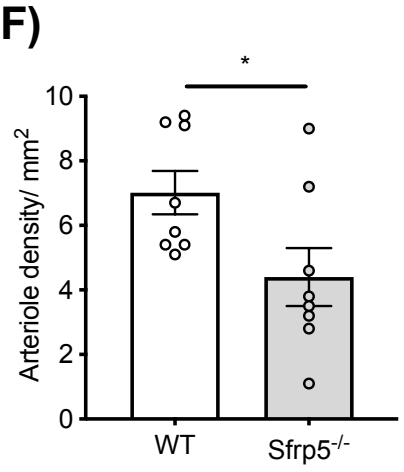
(F)
Arteriole density/ mm2
10
8
6
4
2
0
*
WT
Sfrp5-/-

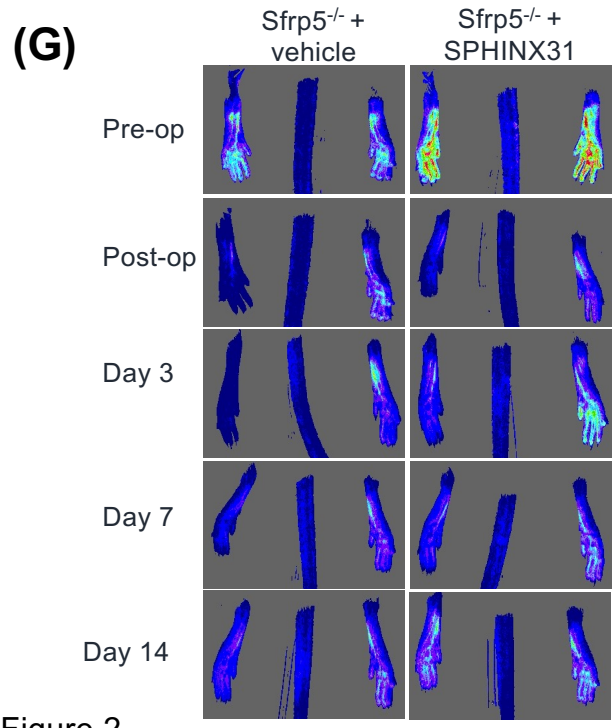
(G)
Sfrp5-/- + vehicle
Sfrp5-/- + SPHINX31
Pre-op
Post-op
Day 3
Day 7
Day 14

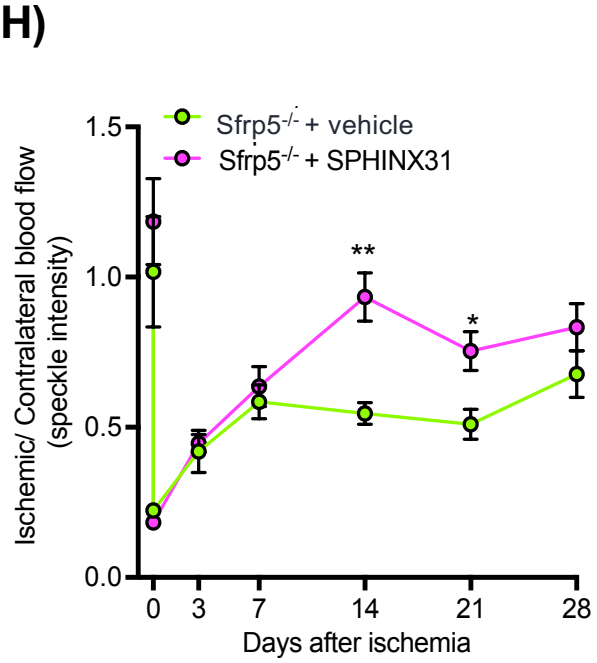
(H)
Sfrp5-/- + vehicle
Sfrp5-/- + SPHINX31
Ischemic/ Contralateral blood flow (speckle intensity)
1.5
1.0
0.5
0.0
0
3
7
14
21
28
Days after ischemia
**
*

Figure 2

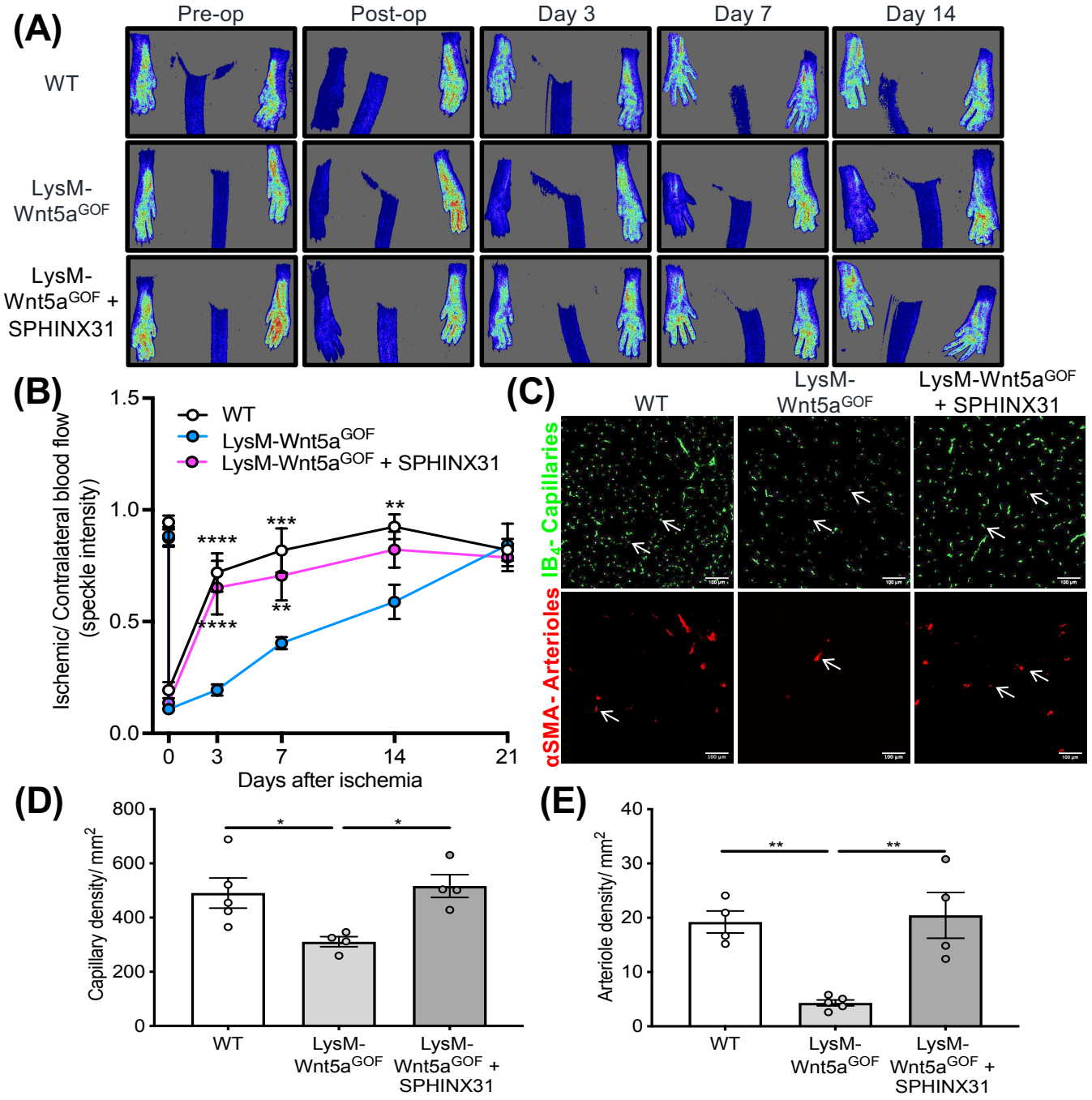
(A)
Pre-op
Post-op
Day 3
Day 7
Day 14
WT
LysM-Wnt5a^{GOF}
LysM-Wnt5a^{GOF} + SPHINX31
(B)
Ischemic/ Contralateral blood flow (speckle intensity)
WT
LysM-Wnt5a^{GOF}
LysM-Wnt5a^{GOF} + SPHINX31
Days after ischemia
(C)
WT
LysM-Wnt5a^{GOF}
LysM-Wnt5a^{GOF} + SPHINX31
IB$_4$- Capillaries
αSMA - Arterioles
(D)
Capillary density/ mm^2
WT
LysM-Wnt5a^{GOF}
LysM-Wnt5a^{GOF} + SPHINX31
(E)
Arteriole density/ mm^2
WT
LysM-Wnt5a^{GOF}
LysM-Wnt5a^{GOF} + SPHINX31

Figure 3

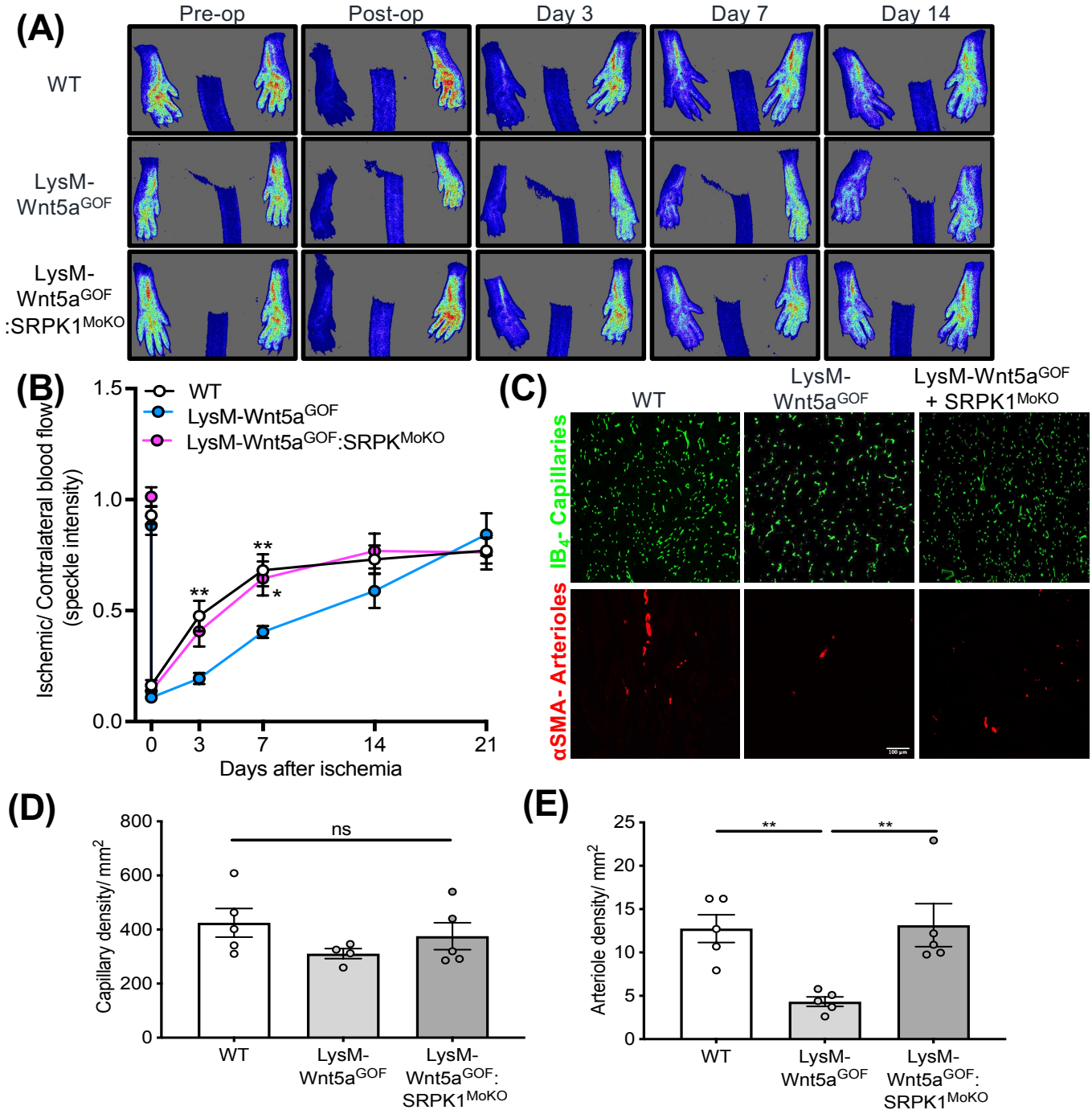
(A)
Pre-op
Post-op
Day 3
Day 7
Day 14
WT
LysM-Wnt5a^{GOF}
LysM-Wnt5a^{GOF}:SRPK1^{MoKO}
(B)
WT
LysM-Wnt5a^{GOF}
LysM-Wnt5a^{GOF}:SRPK^{MoKO}
Ischemic/ Contralateral blood flow (speckle intensity)
Days after ischemia
(C)
WT
LysM-Wnt5a^{GOF}
LysM-Wnt5a^{GOF} + SRPK1^{MoKO}
IB$_4$- Capillaries
αSMA- Arterioles
(D)
Capillary density/ mm^2
ns
WT
LysM-Wnt5a^{GOF}
LysM-Wnt5a^{GOF}: SRPK1^{MoKO}
(E)
Arteriole density/ mm^2
WT
LysM-Wnt5a^{GOF}
LysM-Wnt5a^{GOF}: SRPK1^{MoKO}

Figure 4

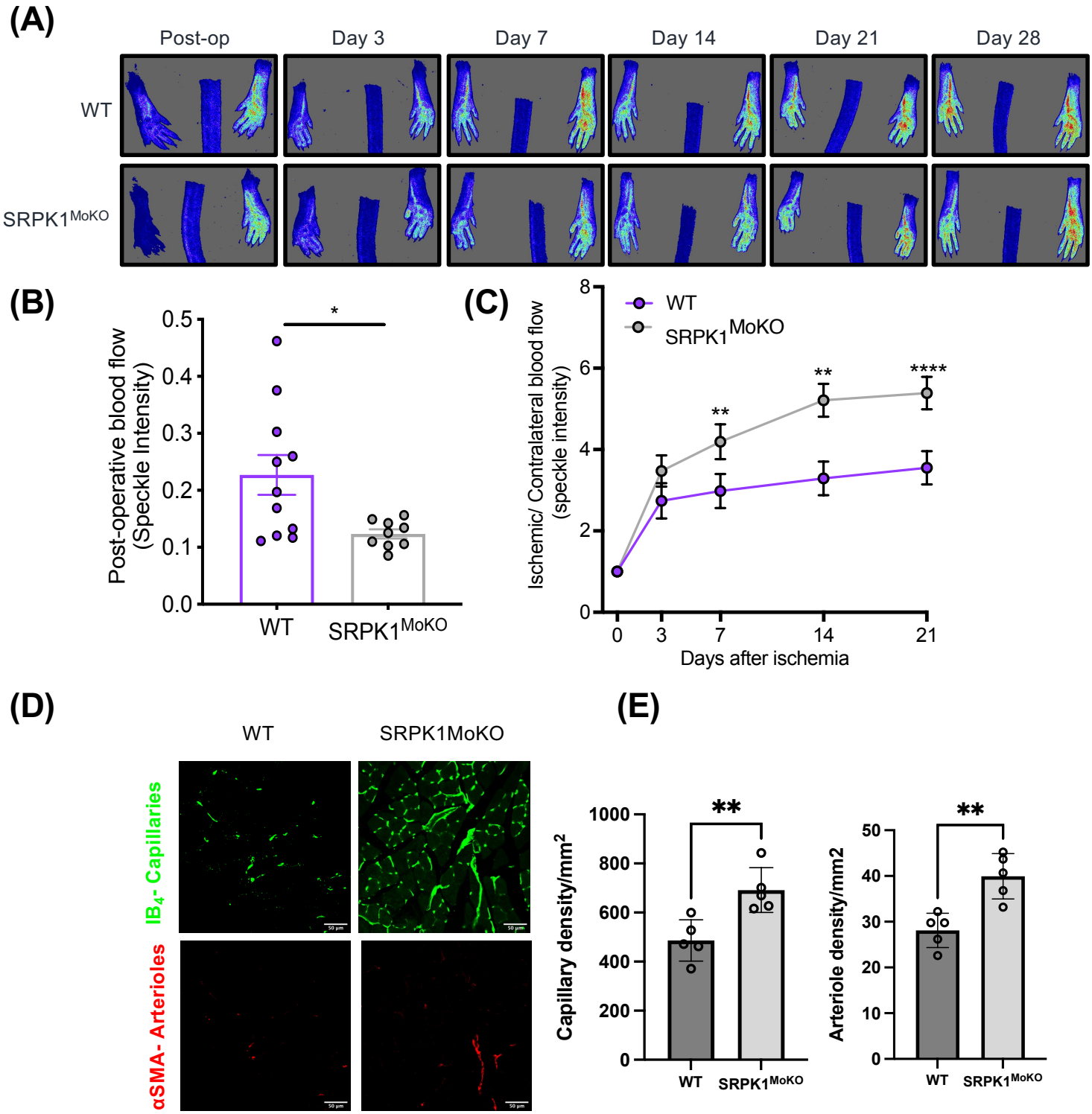
(A)
Post-op
Day 3
Day 7
Day 14
Day 21
Day 28
WT
SRPK1MoKO
(B)
Post-operative blood flow (Speckle Intensity)
0.5
0.4
0.3
0.2
0.1
0.0
*
WT
SRPK1MoKO
(C)
Ischemic/ Contralateral blood flow (speckle intensity)
8
6
4
2
0
WT
SRPK1MoKO
**
**
****
0
3
7
14
21
Days after ischemia
(D)
WT
SRPK1MoKO
IB4- Capillaries
αSMA- Arterioles
(E)
Capillary density/mm2
1000
800
600
400
200
0
**
WT
SRPK1MoKO
Arteriole density/mm2
50
40
30
20
10
0
**
WT
SRPK1MoKO

Figure 5

SUPPLEMENTARY FIGURES

(A)

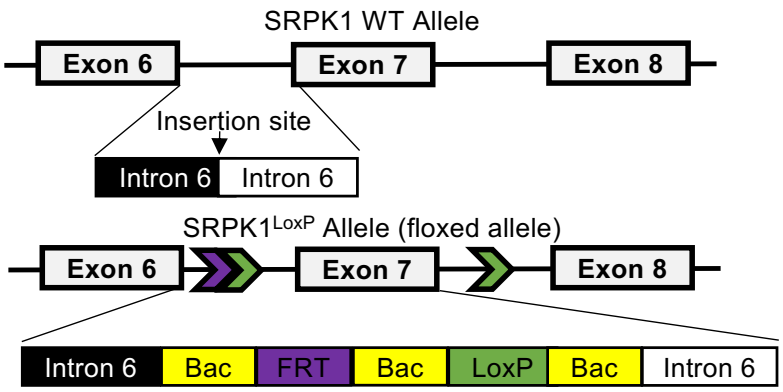

(B)

***Srpk1* expression: RT-PCR**

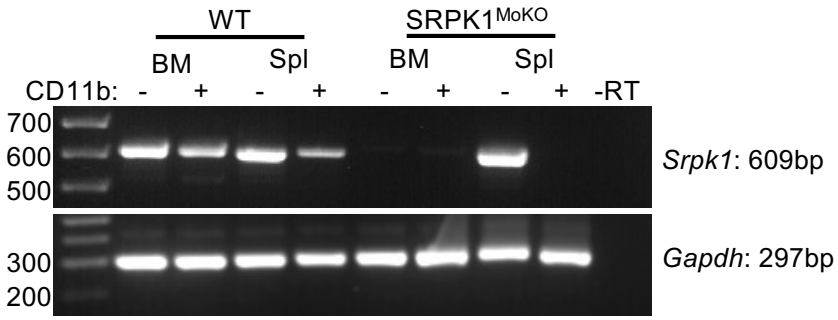

Key: BM= Bone marrow; Spl= Splenocytes

Supp fig 1

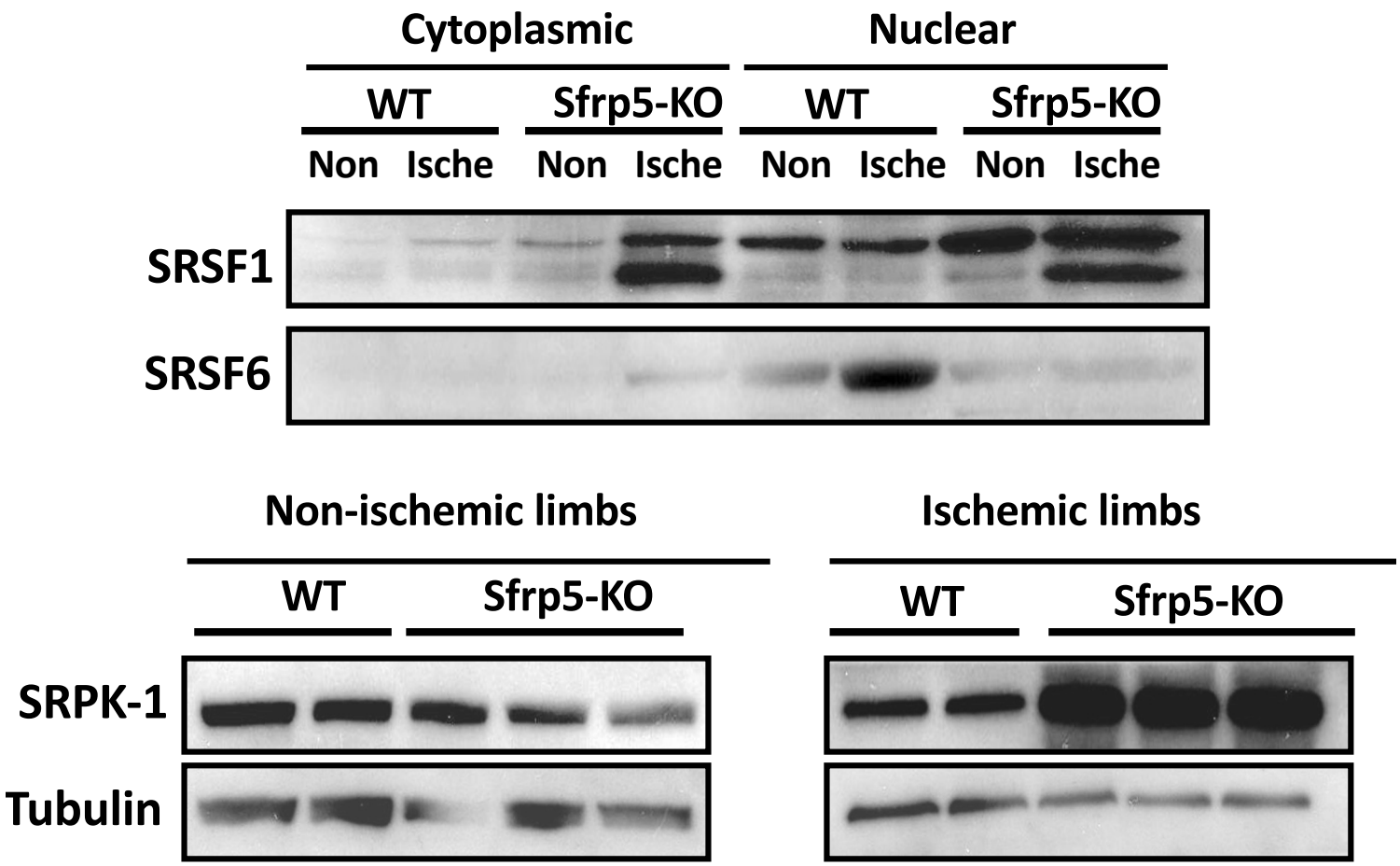
Cytoplasmic
Nuclear
WT
Sfrp5-KO
WT
Sfrp5-KO
Non
Ische
Non
Ische
Non
Ische
Non
Ische
SRSF1
SRSF6
Non-ischemic limbs
Ischemic limbs
WT
Sfrp5-KO
WT
Sfrp5-KO
SRPK-1
Tubulin

Supp fig 2